RSC Advances

ROYAL SOCIETY OF CHEMISTRY

www.rsc.org/advances

The exfoliated graphite as fillers to improve poly(phenylene sulfide) electrical conductivity and mechanical property

Maliang Zhang, Haixia Wang, Zhenhuan Li* and Bowen Cheng*

School of Materials and Chemical Engineering, The State Key Laboratory of Hollow Fiber Membrane Materials and Processes, Tianjin Polytechnic University, Tianjin, 300160, China

*Corresponding author. Tel.: +86 022 83955358; Fax: +86 022 83955055
E-mail address: Zhenhuanli1975@aliyun.com (Z.H.Li); Bowen15@tjpu.edu.cn (B.W. Cheng).

ABSTRACT

Electrical conductive poly(phenylene sulfide) (PPS)/exfoliated graphite (EG) composites were prepared by 1-chlornaphthalene blending method, and the interface effects of EG and PPS on PPS/EG properties were characterized. EG was an excellent nanofiller for enhancing composite conductivity, and PPS/reduced exfoliated graphite oxide (REGO) composite displayed the better conductivities in the range from 3.42×10^{-3} to 1.17×10^{-2} S/cm as REGO loading increase from 0.5 to 5 wt%. However, PPS/exfoliated graphite oxide (EGO) exhibits the much lower conductivity than composite reinforced with REGO. EGO can be well dispersed into PPS matrix, but the oxygen-containing carbons introduce structural defects on EGO surface that disrupt the electronic continuum medium and reduce electrical conductivity. However, the incorporated EGO can effectively improve the mechanical properties of PPS, but REGO displays very poor capacity to enhance PPS mechanical performance. When EGO concentration reached 1 wt%, the breaking strength of PPS/EGO achieved the maximum 1.3×10^{3} MPa, and this value was 109.5 time as that of PPS, The excellent mechanical properties of PPS/EGO were mainly attributed to the heterogeneous nucleation of EGO and the formation of a large number of covalent bond by EG-thiol adducts.

Introduction

In the past decade, polymer composites have been dominant in the materials world, in which the discrete constituents on the order of a few nanometers are incorporated in the polymer matrix.[1, 2] It has been established that the utility of nanofillers could enhance the mechanical, thermal and electrical properties of polymers. PPS is an attractive engineering thermoplastic that is widely used in practice due to its excellent properties.[3-5] The enhancement in PPS polymer properties has been reported with the addition of microscaled and nanoscaled fillers, such as single-walled carbon nanotubes (SWCNTs),[6, 7] inorganic fullerene-like tungsten disulfide (IF-WS_2),[8] SWCNT-IF-WS_2,[9-11] functionalized SWCNTs and Multi-walled carbon nanotubes (MWCNTs), [12-15] Titanium dioxide (TiO_2), zinc oxide (ZnO), cupric oxide (CuO) and silicon carbide (SiC),[16] nanoscale alumina particles,[17] graphite,[18] glass fiber,[19] metal inorganic salt,[20] nano-SiOx [21] carbon and fiber [22] et al. The properties of PPS based composites hardly increase at low nanofiller loadings (up to 1 wt%), [9, 23, 24], and the nanofiller-reinforced composites require homogenous filler dispersion and good interfacial adhesion with the host matrix to improve the performance of PPS. However, the dispersion processing is hindered by the poor solubility of nanofiller and their strong agglomerating tendency.[25] Attaching functional groups onto the filler surface has been proven to be an effective approach to prepare polymer composites, and another effective way to achieve this goal is to wrap filler by organic polymers that provide the possibility for π-π stacking interactions with the nanofiller sidewalls, [7] In addition, the naofiller type, degree of

dispersion and interfacial adhesion with the matrix have strong influence on the properties of PPS based composites.

Graphene is an atomically thick, two-dimensional (2-D) sheet which composed of sp^2 carbon atoms and arranged in a honeycomb structure.[26] Graphene has been widely studied as the outstanding candidates to incorporate into polymer materials by researchers, due to its unique two-dimensional structure and extraordinary properties, such as heat conductivity, high electronic mobility and quantum effects.[27] For example, PPS/graphene composites have significantly improved thermal conductivity as compared with the neat polymer.[28, 29] However, the graphene filler for improving PPS electrical conductivity has not been reported, and graphene is difficult to be well dispersed into polymer matrix because graphene layers usually easily self-aggregate due to the intrinsic van der Waals force.[30]

The goal of this paper is to prepare electrical conductive PPS/EG composites, and the interface effects between EG and PPS on PPS/EG material properties were characterized by transmission electron micrographs (TEM), X-ray diffraction (XRD), fourier transform infrared spectra (FT-IR), X-ray photoelectron spectroscopy (XPS), differential scanning calorimetry (DSC), thermogravimety (TG), field emission scanning electron microscopy (FESEM), single fiber strength tester technology and four-point probe method. The influence of EG structure on filler dispersion, EG interfacial adhesion with the host matrix, composite thermal properties, PPS electrical conductivity and mechanical property were investigated to correlate the microscopic structure with macroscopic properties.

Materials and methods

Materials

PPS (Mw=3.3×10^4, Mw/Mn=1.4, d25^{o}C ~ 1.35 g/cm^3, Tg ~ 90 ^{o}C, Tm~ 280^{o}C) was synthesized from Na_2S and 1,4-dichlorobenzene in N-methylpyrrole (the mole ratio of Na_2S to 1,4-dichlorobenzene ~ 1.01), The end groups of synthesized PPS contained SH and PhCl. 1-chlornaphthalene (95%, Fluka) was purchased from J&K Chemical Co., Ltd and purified by distillation under reduced pressure before use. Natural graphite powder (80 mesh) was supplied by Tianjin Chemical Co., Ltd and used as received. $KMnO_4$ (99.5%), H_2SO_4 (98%), HCl (35%), $NH_3 \cdot H_2O$ (25%, aq.), hydrazine hydrate ($H_4N_2 \cdot H_2O$, 80%, aq.) and $NaNO_3$ (99.8%) et al were purchased from Tianjin Kermel Chemical Reagent Co., Ltd.

Characterization

The chemical states of C atom were characterized by XPS (ThermoFisher K-alpha). FT-IR was measured through a TENSOR 37 (BRUKER Corporation, Germany) and operated by attenuated total reflectance (ATR) in the wavenumber range of 4000-500 cm^{-1}. TG (STA409 PC thermogravimety, NETZSCH, Germany) measurement was carried out from 30 to 900 ^{o}C at a heating rate of 10 ^{o}C /min under an air atmosphere. XRD analysis was conducted using an Elmer PHI-5600 using an Mg Kα line as a radiation source and a D8 Discover. The morphology of composites was characterized by a FESEM (Hitachi 4800S, and Japans) and TEM (Hitachi H-7650 microscope). DSC analysis was performed on a Perkin Elemer DSC-7 under nitrogen condition, and samples placed in aluminium pans were melted at 320 ^{o}C and

kept at this temperature for 5 min to erase their thermal history. Subsequently, they were cooled from the melt to room temperature and then heated again up to 320 ^{o}C at 10 ^{o}C/min. From the DSC heating and cooling traces, peak melting temperature (T_m), heat of melting (ΔH_m), peak crystallization temperature (T_c) and heat of crystallize (ΔH_c) were obtained. The degree of crystallinity (X_c) was calculated from the following equation:

$$X_c(\%) = \frac{\Delta H_c}{\Delta H_f (1 - W_f)} \times 100\% \qquad (1)$$

Where ΔH_c is the cold crystallization enthalpy from the DSC scan, W_f is the weight fraction of C_{60} in composites, and ΔH_f is the melting enthalpy of 100% crystallized PPS which was taken as 105J/g.[18] The breaking strength (δ_t), breaking elongation (ε) and tensile modulus (MPa) of PPS/EG fibers were measured on single fiber strength tester (China LLY-06). Each sample was tested ten times to evaluate the average value. The breaking strength was calculated from the following equation:

$$\delta_t (MPa) = 4 \frac{F_b}{\pi d^2} \times 10^{-6} \qquad (2)$$

Where F_b is the maximum tension value, d is the fiber diameter. The breaking elongation was determined by the following equation:

$$\varepsilon(\%) = \frac{L - L_0}{L_0} \qquad (3)$$

Where ε is the breaking elongation, L is the length of fiber elongation, L_0 is the initial length of the fiber before test. The fiber tensile modulus (E MPa) was determined by the following equation:

$$E = \frac{\delta_t}{\varepsilon} = \frac{4F_b L_0}{\pi d^2 (L - L_0)} \times 10^{-4} \qquad (4)$$

Electrical conductivity at room temperature was measured by the four-point probe method using a Scientific Equipment device with a spacing probe S = 0.2 cm equipped with a DC precision power source (Model LCS-02) and a digital microvoltmeter (Model DMV-001).[12]

Sample Preparation

EGO is synthesized according to Hummers method.[20] 5.0 g graphite, 2.5 g $NaNO_3$, and 100ml H_2SO_4 were loaded in a 1000-ml round-bottom flask with magnetic stirring. After being cooled with ice-water bath at 0-3 °C for 1h, 15.0 g $KMnO_4$ was added into above reaction system. After reaction was kept at 0-5 °C for 1h and then heated at 35 °C for 2h, the mixture was diluted with 600 ml deionized water and reacted at 90 °C for 15 min. 50 ml deionized water and 18 ml H_2O_2 (30%) were added into above suspension under the condition of magnetic stirring. After filtration, purification and dry, EGO was obtained.

EGO was reduced to REGO by hydrazine in an aqueous ammonia solution. After 3.0 g EGO and 300 ml deionized water were loaded in a 500 ml three-neck flask, 20 ml ammonia and 6 ml hydrazine were respectively loaded into above suspension which undergoes ultrasonication, and then the system was heated at 95 °C for 24 h under the condition of magnetic stirring. The obtained REGO was washed with deionized water, and it was dried at 50 °C for 12 h under vacuum condition.

PPS was dissolved in 1-chlornaphthalene at 205 ^oC, and 0.05 to 5 wt % EGO or REGO were loaded into above described solution. The suspension was kept at 205 ^oC

for 3 h under the condition of stirring. PPS/EGO or PPS/REGO composites were obtained after removing the dissolvent by alcohol extraction and evaporation under vacuum condition. Fibers (d~0.003 mm) were prepared from PPS/EGO or PPS/REGO composites on the self-made fiber instrument at 310 ^{o}C. The prepared PPS/EGO or PPS/REGO fibers were pretreated at 90 ^{o}C H_2O for 2 hours, and then the prepared specimen was tested or characterized on LLY-06 tensile tester at room temperature.

Results and discussion

TEM images of EGO and REGO

Fig. 1 showed TEM images of EGO (Fig. 1 a) and REGO (Fig. 1 b). The planar sheets are observed clearly in both EGO and REGO, and the feature of high surface/volume ratio and two-dimensional structure of EGO morphology are well maintained, however REGO appears agglomerate.

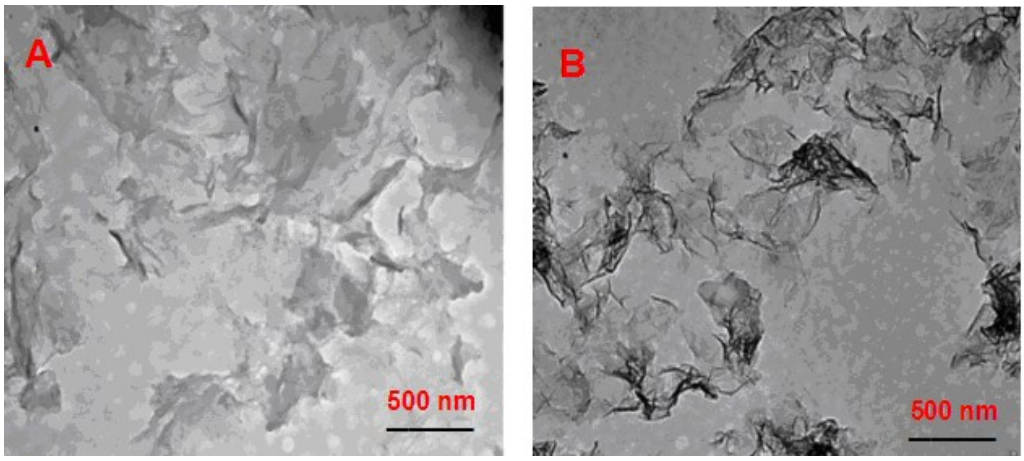

Fig. 1 TEM images of EGO and REGO

XRD patterns of composites

Fig. 2 shows a XRD pattern of EGO with a characteristic (002) peak at 2θ= 10.5°, having an interlayer distance of ~0.9 nm. The oxygen functional groups

attached to both sides of the graphite flakes to create atomic defects (sp3 bonding) in the graphite structure, and graphite flakes tend to be exfoliated to a few layers or individual layers in an aqueous medium.[31] As for REGO, the complete disappearance of the strong (002) peak suggests the successful reduction of EGO. A new peak at 26.3° (2θ) was detected, which is a clear indication of the planar sheet agglomeration by π-π stacking interactions.[32, 33]

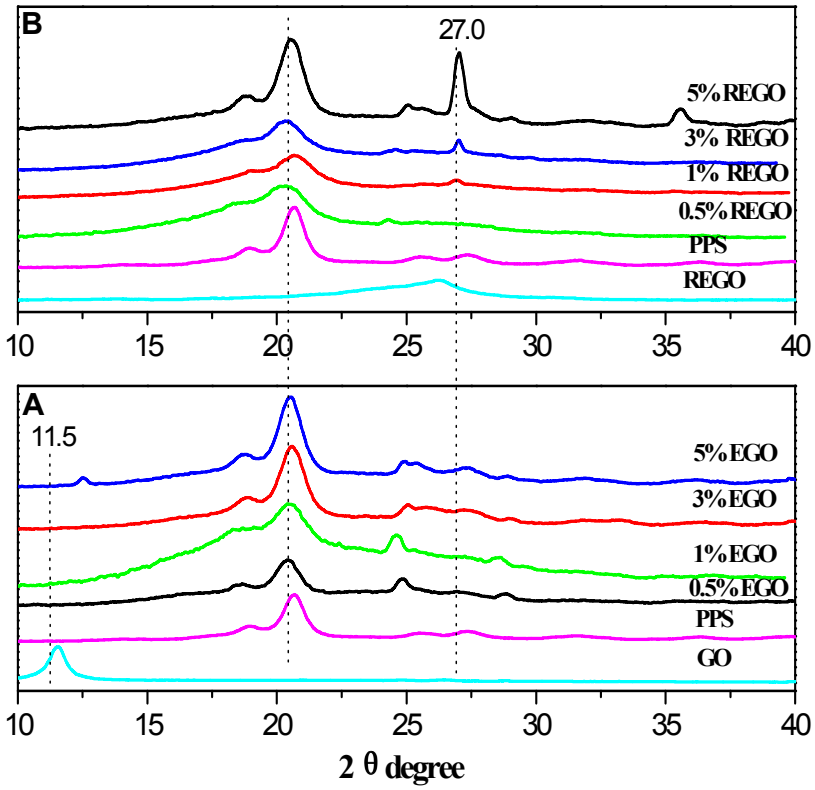

Fig. 2. A: XRD patterns of PPS, EGO and PPS/EGO composites, B: XRD patterns of PPS, REGO and PPS/REGO composites.

As shown in Fig. 2 A, the two diffraction peaks at 19.5° and 21.5° are corresponding to the (110) and (200) planes of orthorhombic structure of PPS.[34] EGO was not detected in composites with EGO content less than 5 wt%, implying that

EGO can be well dispersed. When EGO content comes up to 5 wt%, a new weak diffraction peak at 12.5° appeared which indicated PPS and EGO might exist a great interaction to result in EGO lattice deformation. As shown in Fig. 2 B, REGO has a weak broad diffraction peak at 26.5°, and it do not appear in composites with 0.5 wt% REGO content. However, when REGO content came up to 1 wt%, a new diffraction peak at 27.0° appeared which demonstrated REGO easier reunion and more difficult dispersion. In addition, the intensity of PPS characteristic diffraction peaks distinctly decreased after doping with REGO, which was significantly deferent from the results of PPS/EGO.

FT-IR spectra of composites

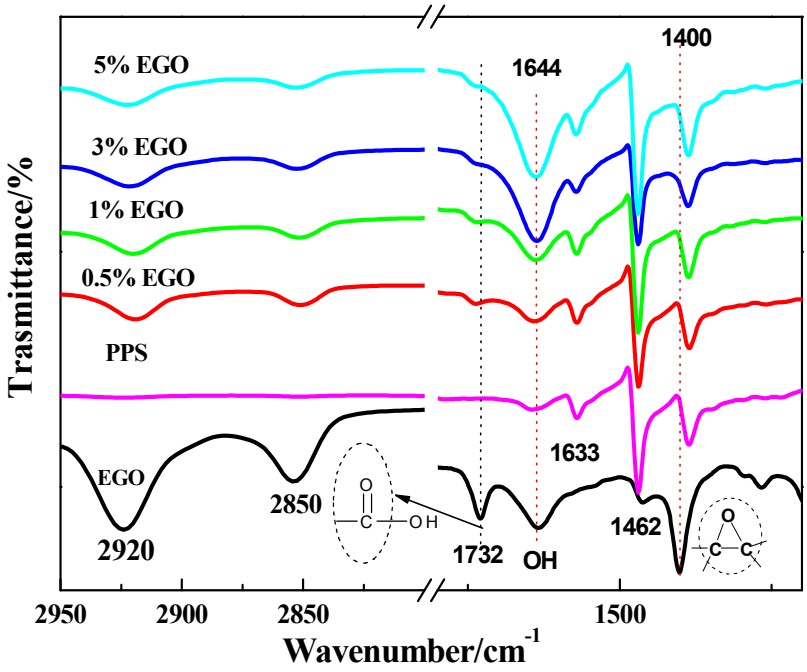

Fig. 3. FT-IR spectra of PPS, EGO and PPS/EGO composites

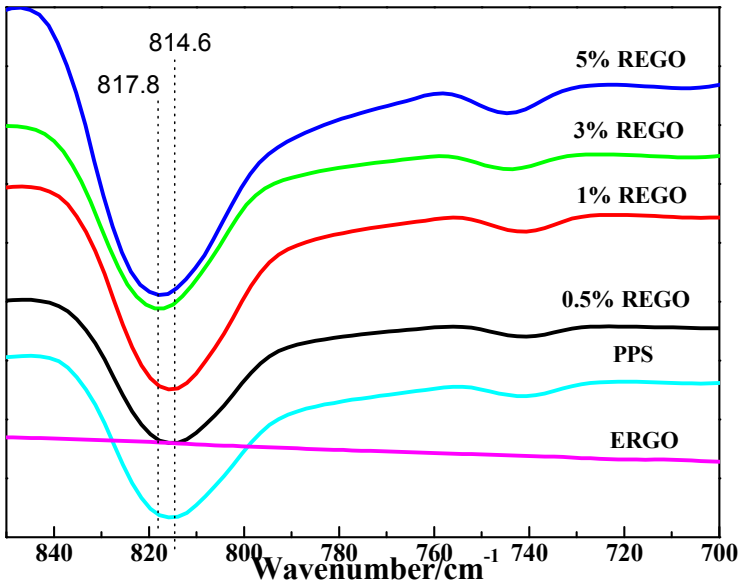

Fig. 4. FT-IR spectra of PPS, REGO and PPS/REGO composites

In order to explore the interaction between PPS and EG (EGO and REGO), PPS/EGO and PPS/REGO were characterized by FT-IR (Fig. 3 and 4). The absorption peaks at 1573, 1472, 1390, 1011 and 554 cm^{-1} are PPS characteristic absorption peaks, and two bands appear at 1011 and 554 cm^{-1} were attributed to aromatic C-S stretching vibrations.[35] The bands at 2920-2850 (CH), 1732 (C=O) and 1462 cm^{-1}(C-O) are EGO characteristic absorption peaks [22]. REGO characteristic absorption peaks appeared at 2920-2850 (-CH) and 1640 cm^{-1},[36, 37] and nearly no carbonyl peak at 1732 cm^{-1} was detected. After PPS was doped with EGO, the EGO characteristic absorption peaks (epoxy groups) at 1462 cm^{-1} disappeared, at same time PPS/EGO display an intensive absorption peaks (OH species) at 1644 cm^{-1}. However, when PPS was doped with REGO, REGO and PPS remained their respective characteristic absorption peaks. In summary, the disappearance of 1462 cm^{-1} peak and the intensity increase of 1644 cm^{-1} peak implied the thiol adducts took place by reacting EGO with excessive PPS

(Fig.5). It is general known that the formation of π-π stacking interactions can be characterized through the shift of –CH bond. In PPS/REGO material, the C-H bond absorption peaks of PPS located at 814.6 cm^{-1}, while C-H vibration peak of 5 wt% PPS/REGO shifted to 817.8 cm^{-1}, which indicated that there existed a strong π-π stacking interactions between REGO and PPS matrix.

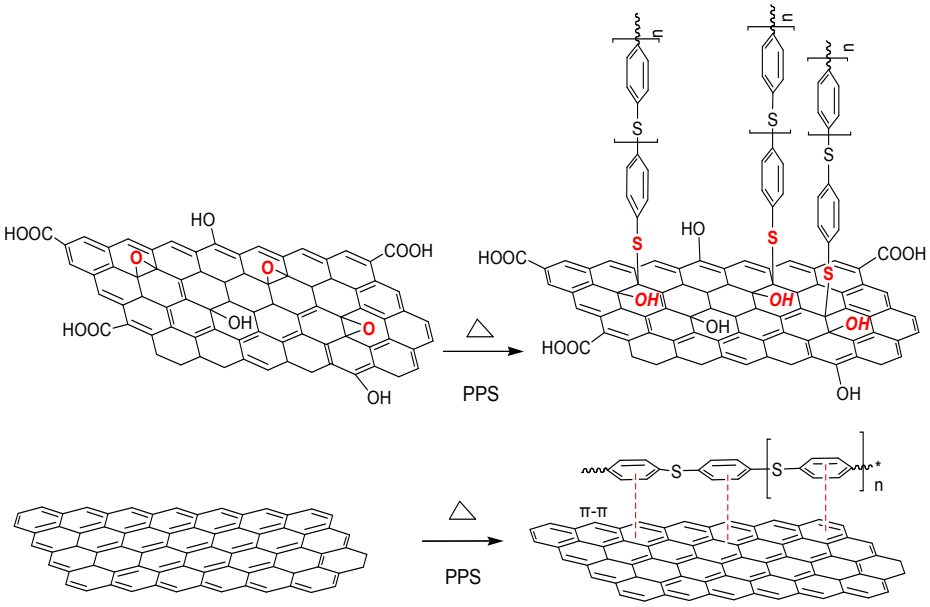

Fig. 5. The interaction between PPS and EG (EGO and REGO)

XPS analysis of composites

Fig. 6, Fig. 7 and Fig. 8 showed XPS spectra of EGO, REGO, PPS/EGO and PPS/REGO. The absorption peak at 284.7 eV is PPS characterized absorption peak. EGO represented four kinds of oxygen-containing carbons: carbon-hydroxyl groups (C-OH) at 285.7 eV, epoxy/ether groups (C-O) at 286.7 eV, carbonyl groups (C=O) at 288.0 eV and carboxylate carbon group (O-C=O) at 289.4 eV, in addition to nonoxygenated C at 284.5 (Fig. 6.a).[38-41] As for PPS/EGO composites, C1s electron

binding energy of PPS/EGO significantly increased as EGO concentration rising, e.g., C1s electron binding energy of 5 wt% PPS/EGO indicated that C(O)O, C=O and C-O groups appeared. Those results demonstrated EGO successful incorporation into PPS or EGO filler agglomeration on the surface of composites, which is in agreement with FT-IR spectra (Fig. 3).

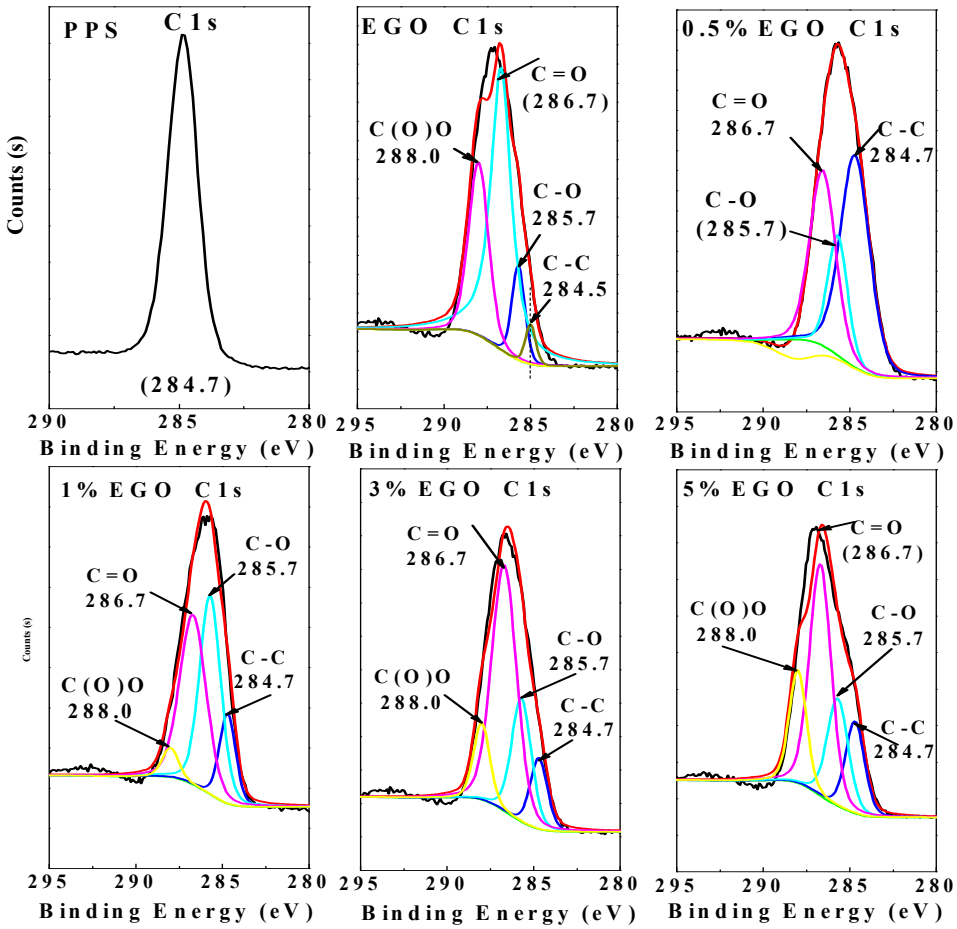

Fig. 6. XPS analysis on the C 1s curves of pure PPS, EGO and PPS/EGO composites.

The oxygen peak was almost completely suppressed after the reduction process by chemical reducing agents (NH_2-NH_2), and the C 1s XPS of REGO showed only a little of C(O)O, C=O and C-O groups remaining on the REGO (Fig. 7). REGO

addition significantly decreased the C1s electron binding energy of C-C, e.g., C1s electron binding energy of 5 wt% PPS/REGO showed that a few C=O and C-O groups occurred, which exhibited REGO successful incorporation into PPS or REGO filler agglomeration on the surface of composites. Also, the wide scan of XPS analysis to show the related peaks for C, O and S was listed in Fig.8. The characterized peaks of PPS and ERGO or EGO appeared in their corresponding composites.

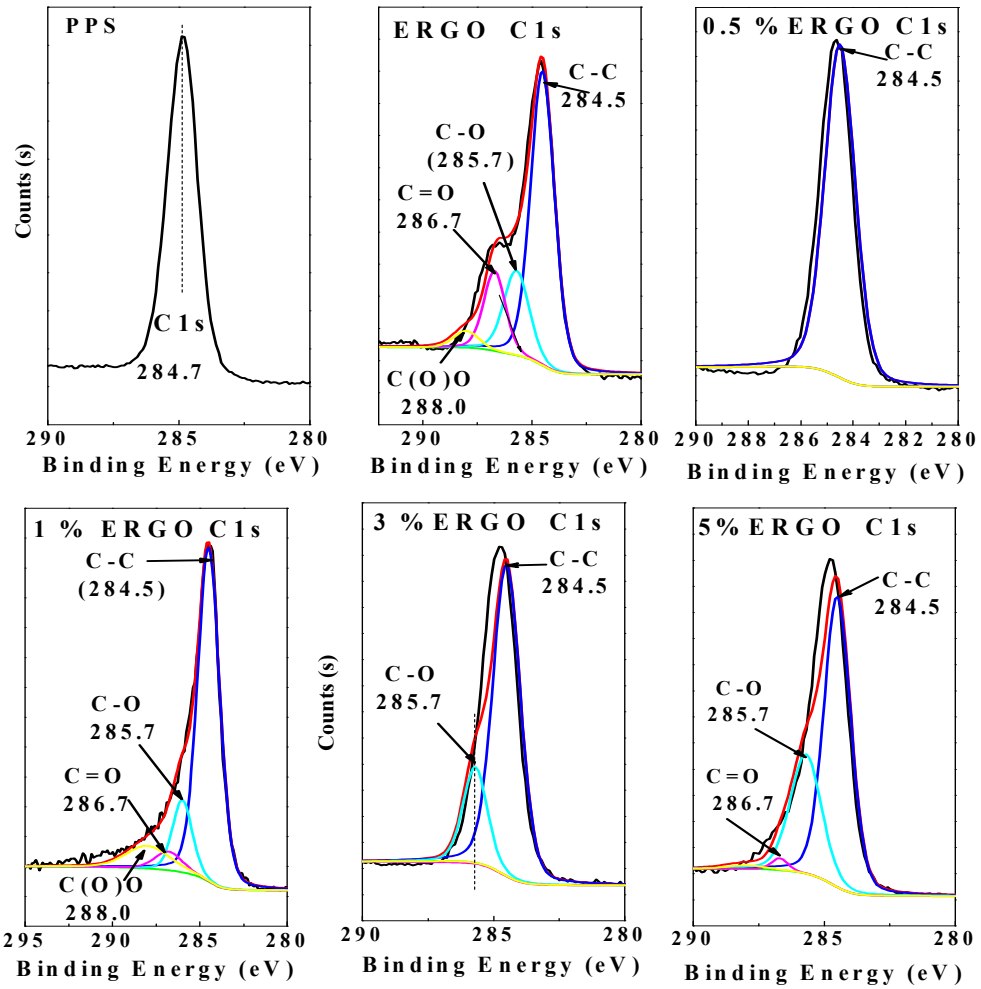

Fig. 7: XPS analysis on the C 1s curves of pure PPS, REGO and PPS/REGO composites.

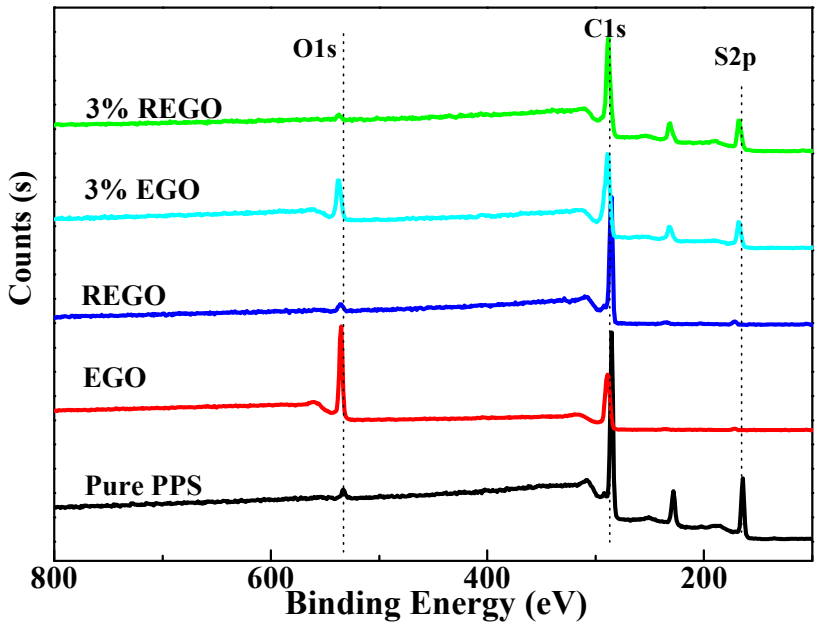

Fig. 8: The wide scan of XPS analysis for C, O and S.

DSC heating scans and cooling scans for composites

Thermal analysis is a powerful tool for characterizing the physical–chemical properties, and the melting behavior and crystallization process of composites were further studied by DSC (Fig. 9 and Fig.10). PPS presented the onset temperature of melting (T_{mo}) at 270 ^{o}C and the peak melting temperature (T_m) at 280 ^{o}C. The addition of EGO into PPS has a little influence on T_{mo} and T_m, however, PPS/REGO exhibit a multiple melting behavior. Those behaviors may result from the variation in morphology (such as lamellar thickness, distribution, perfection or stability) or the relaxation of the rigid amorphous fraction. As shown in Fig. 10 A, When PPS was modified with EGO, an obvious change of the onset temperature of crystallization (T_{co}) and peak crystallization temperature (T_c) were observed. T_{co} and T_c of PPS/EGO significantly increased as EGO loading rising, e.g., T_{co} and T_c of 3 wt% PPS/EGO

were 252.2 °C and 243.5 °C, both higher than that of PPS. However, much more EGO loading caused the decrease of T_{co} and T_c, e.g., T_{co} and T_c of 5 wt% PPS/EGO declined to 243.8 °C and 236.1 °C. In Fig. 10B, the Tc is the smallest when the ERGO content is 0.5wt%. The π-π stacking interactions between ERGO and PPS matrix hinders polymer chain diffusion during crystallization, resulting in crystallization temperature decrease. However, as ERGO filler content increase, PPS nonisothermal cold crystallization is enhanced by ERGO, indicating that ERGO also plays a role on heterogeneous nucleating. For example, T_{co} and T_c of 3 wt% PPS/REGO increased to 240.1 °C and 219.5 °C.

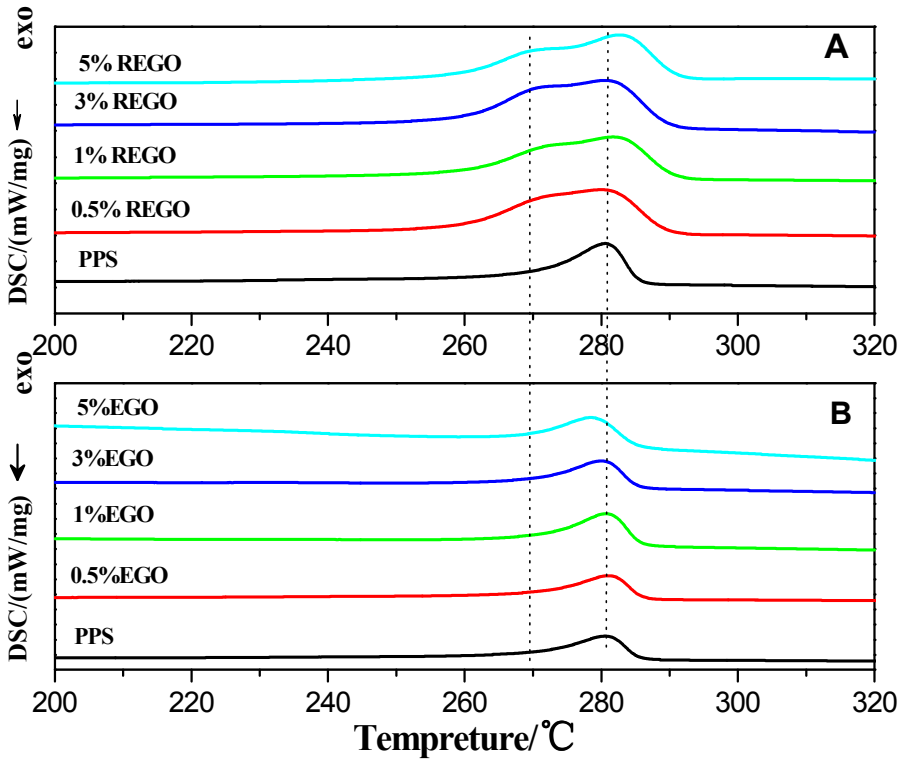

Fig.9. A: DSC heating scans for PPS and PPS/REGO composites, B： DSC heating scans for PPS and PPS/EGO composites

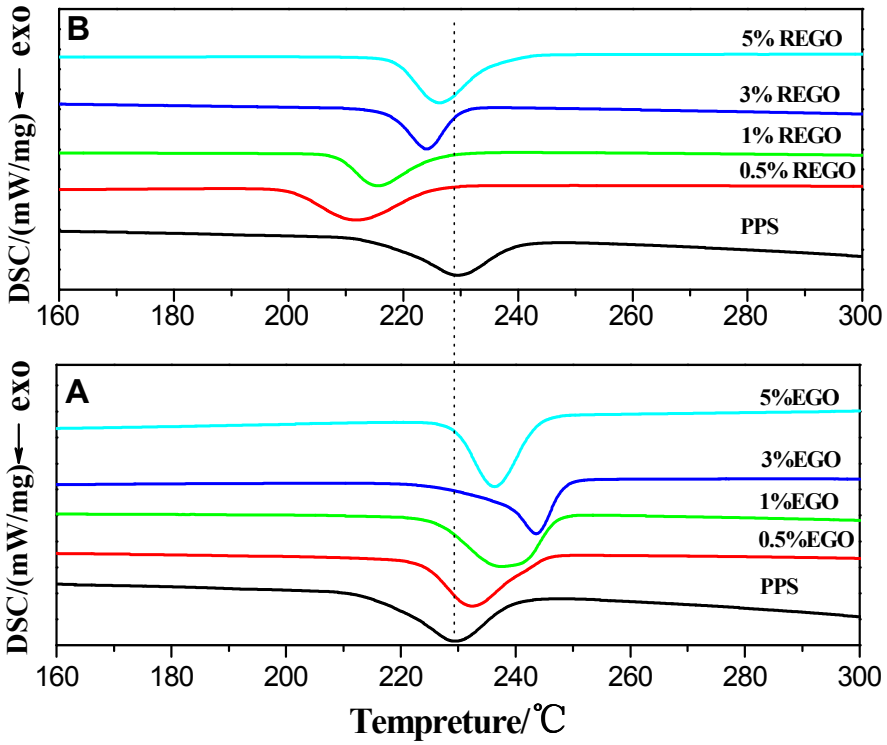

Fig.10. A: DSC cooling scans for pure PPS and PPS/EGO composites, B: DSC cooling scans for pure PPS and PPS/REGO composite

Generally, the addition of EGO has two opposite effects on crystallization properties. On the one hand, fillers promote the nucleation of PPS. On the other hand, fillers hinder the mobility and diffusion of PPS chains, which results in a slower crystallization rate than that observed in PPS.[42, 43] When EGO content is less than 3 wt%, composites are easier crystallization, which can be attributed to EGO heterogeneous nucleation. However, when EGO content comes up to 5 wt%, composites are slower crystallization, which was attributed to the mass barrier effect from EGO or the intense restrictions on chain mobility from EGO-polymer chemical interactions.[44, 45] It was worthy of noting that the addition of REGO did not well promote PPS heterogeneous nucleation, which is contrary to the results of PPS/EGO.

The great different performance of EGO and REGO in the melting behavior and crystallinity of PPS was attributed to their different interface effects between PPS matrix and fillers. In other words REGO mainly hinders the mobility and diffusion of PPS chains to result in it difficult crystallization[46], while EGO plays a great role on PPS heterogeneous nucleating. Those DSC results were well consistent with XRD characterization.

TGA curves of composites

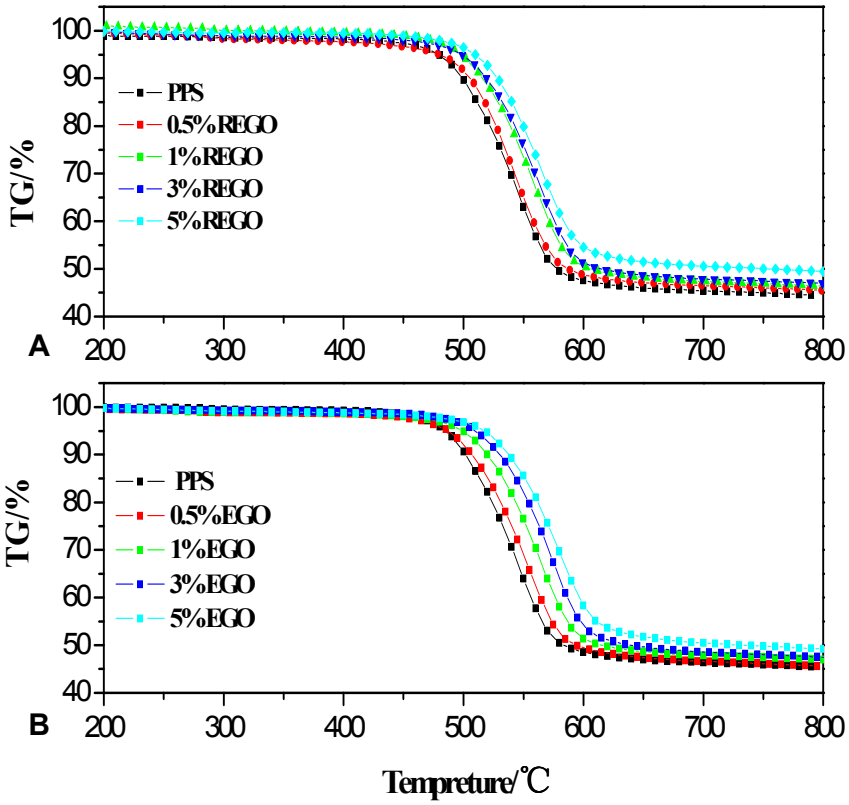

Fig. 11. A: TG curves of PPS, REGO and PPS/REGO composites, B: TG curves of PPS, EGO and PPS/EGO composites

Fig. 11 showed the thermo gravimetric analysis curves of PPS/EGO and PPS/REGO composites. PPS started to lose weight at 475 ^{o}C and was completely decomposed at 580 ^{o}C. Compared with PPS, PPS/EGO and PPS/REGO displayed the

higher initial degradation temperatures, and the residual fraction also increased as filler content rising. Those results are similar to the reported conclusions.[42, 47] By the comparison of PPS/EGO with PPS/REGO, the thermal stability of PPS/EGO was much better than that of PPS/REGO. Such results should be attributed to different factors. EGO fillers are better dispersed within PPS matrix, which restricts chain mobility or diffusion to slow down the decomposition process.[6] The covalent anchoring of PPS to EGO leads to a strong enhancement in the thermal conductivity that facilitates heat dissipation within the composite,[48] which results in longer time for the surface temperature to reach the onset temperature.

SEM observation on EG dispersion in PPS matrix

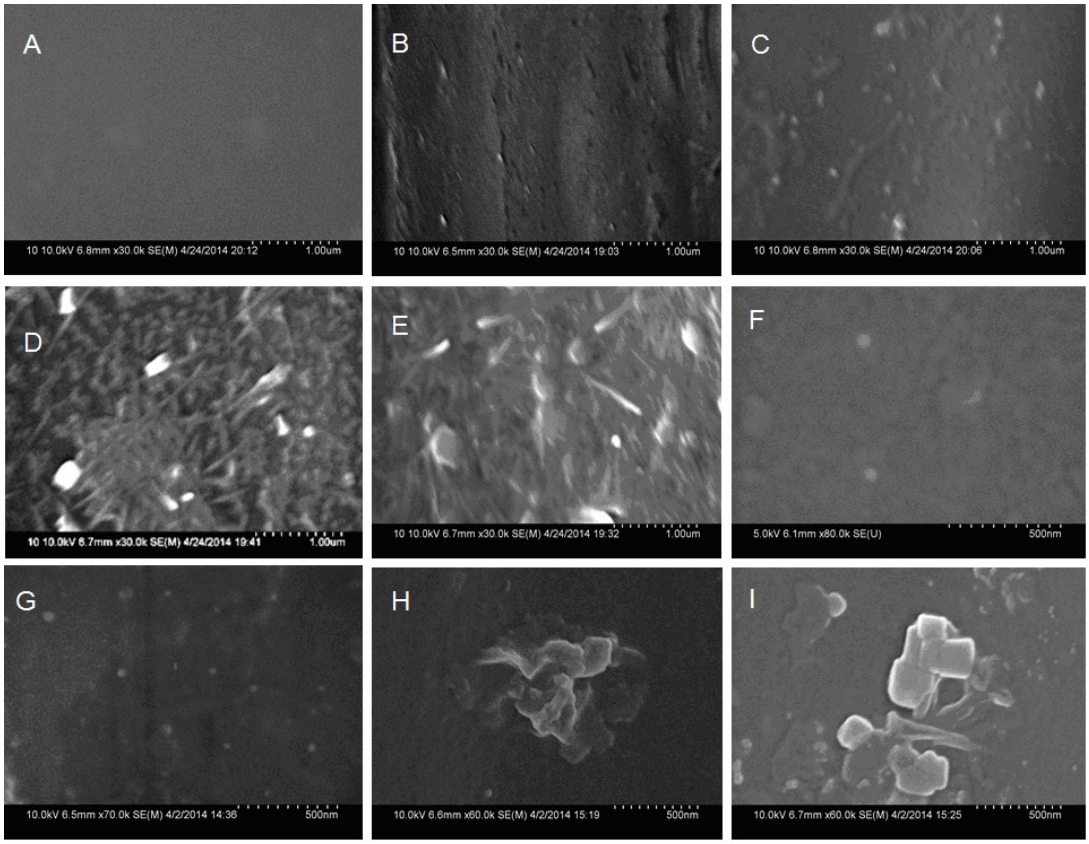

Fig. 12. Surface SEM micrographs of fibers with different weight fractions of EG: (a) PPS; (b) 0.5 wt% EGO; (c) 1 wt% EGO; (d) 2 wt% EGO; (e) 5 wt% EGO; (f) 0.5

wt% REGO; (G) 1 wt% REGO; (H) 2 wt% REGO; (I) 5 wt% REGO

An efficient dispersion of filler in polymer matrix can significantly influence the physical properties of PPS based materials. PPS, PPS/EGO and PPS/REGO fiber surface SEM images were displayed in Fig. 12. The micrograph of 0.5-2 wt% PPS/EGO fibers indicated that EGO was well dispersed into PPS matrix, however, when much more EGO was incorporated into PPS polymer (such as 5wt% PPS/EGO), EGO formed agglomerates on fiber surface. Differ from the SEM surface image of PPS/EGO fibers, the serious REGO reunion were detected in 2-5 wt% PPS/REGO fibers. PPS formed a large number of covalent bonds with EGO which resulted in a tight interfacial layer to improve EGO-matrix interfacial adhesion[49, 50](see Scheme 1). The formation of covalent linkages at the polymer-nanofiller interface can increase the miscibility of EGO with host polymers, and the attaching PPS onto the EGO surface can inhibit filler aggregation.

Mechanical behaviors of PPS/EG fibers

The mechanical behaviors of PPS/EG fibers were investigated by single fiber strength tester technique which provided additional information about filler-matrix and filler-filler interactions. The tensile test charts (Stress vs Strain) for all composites were listed in Fig. 13 and Fig. 14, and Fig. 15 showed the breaking strength, breaking elongation and tensile modulus of PPS/EG fibers. The characterized results indicated that EG concentration had a greater influence on the mechanical performance of PPS/EG fibers. When EGO concentration reached 1 wt%, the breaking strength of composites achieved maximum 1.3×10^3 MPa, and this value was 109.5 time as that of

pure PPS. However, the tensile modulus of hybrid fibers always increased with increasing EGO content. The excellent mechanical properties of PPS/EGO were attributed to EGO heterogeneous nucleation and the formation of a large number of covalent bond by EGO-thiol adducts. However, the excessive EGO addition caused a significant reduction of breaking strength, e.g., the breaking strength of 5 wt% PPS/EGO fiber declined to 624 MPa. The excessive addition of fillers reduced PPS crystallization degree and decreased the combination between PPS and EG, which were attributed to the phenomenon of EGO and REGO aggregation. These results can also confirm by the SEM images of PPS/EG composites (presented in Fig 10). It is expected that the elongation at break must be increased with increasing the concentration of fillers, due to covalent bond between fillers and matrix, but the results don't show that because of the decrease of ductility of the polymer with the incorporation of fillers.[51]

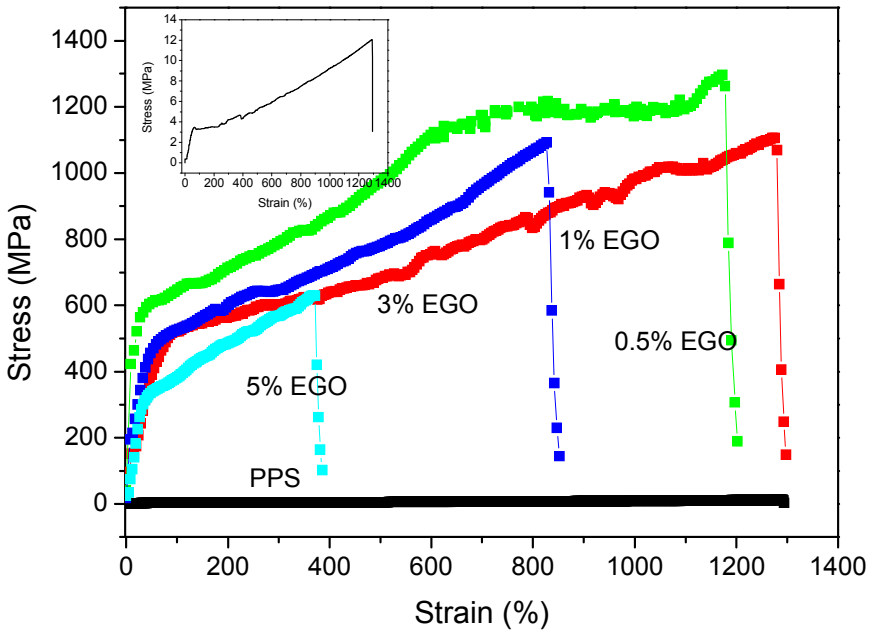

Fig. 13. Tensile test charts of PPS/EGO composites

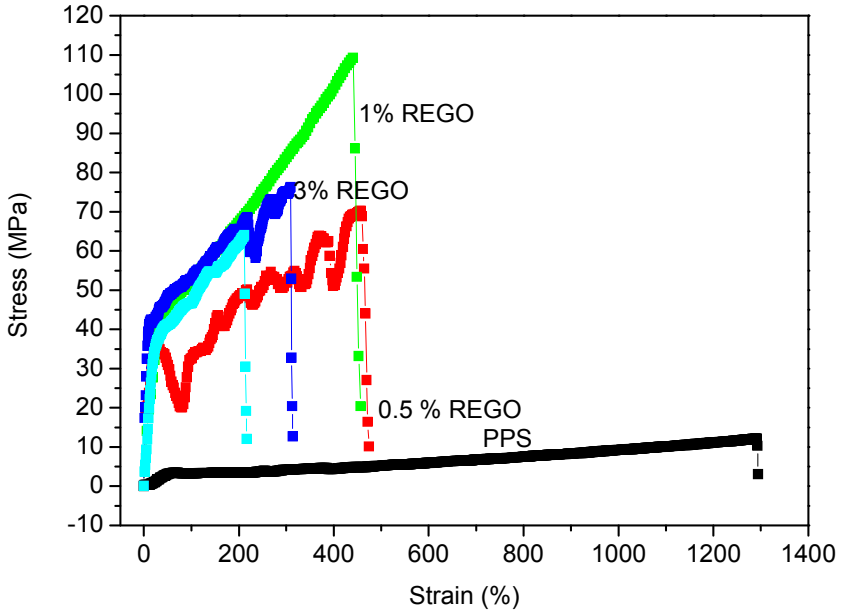

Fig. 14Tensile test charts of PPS/REGO composites

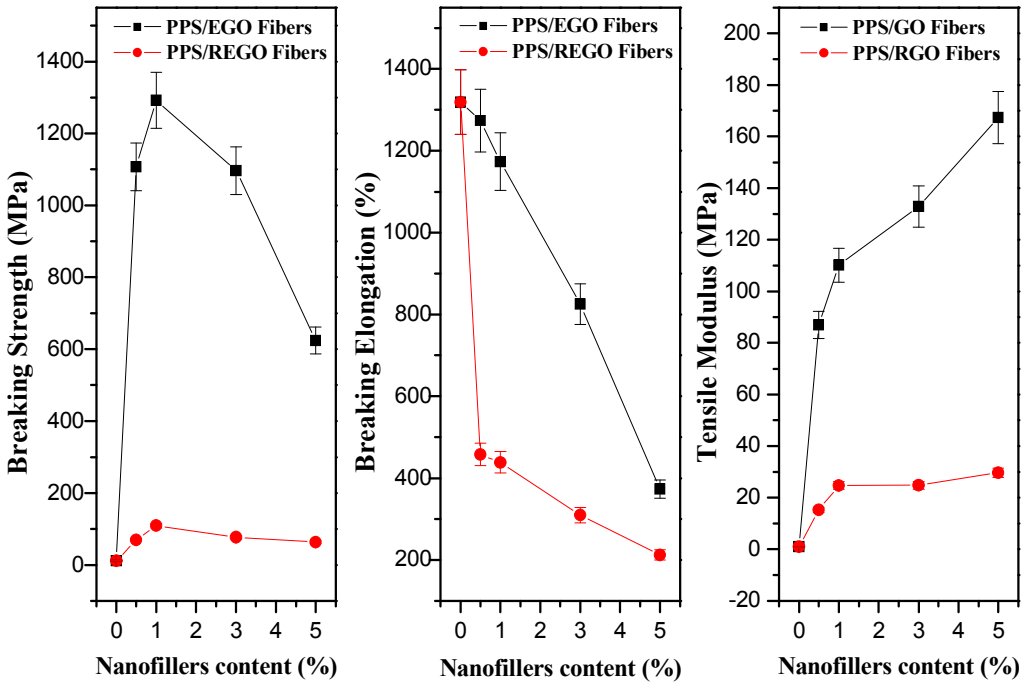

Fig. 15. Mechanical properties of PPS/EG fiber with different filler concentration: (a) breaking strength; (b) breaking elongation; (c) tensile modulus

Electrical conductivity

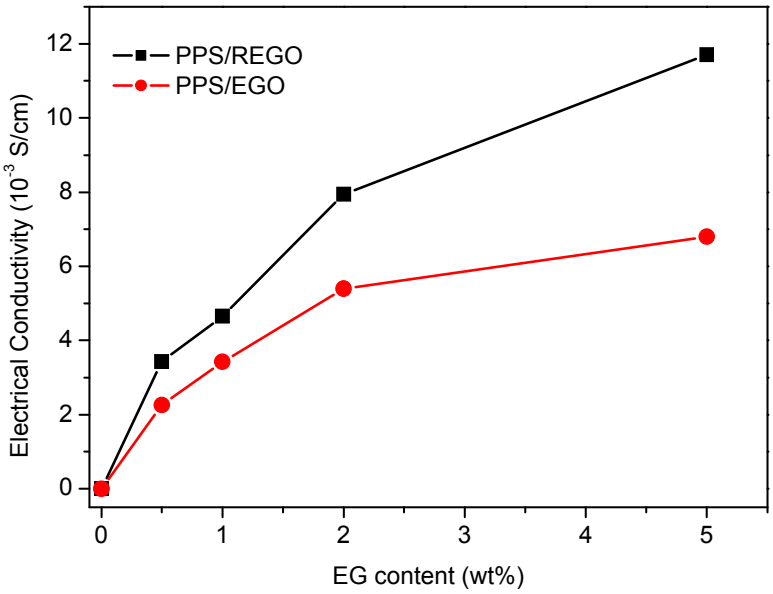

Fig. 16. Room temperature electrical conductivity of PPS/EGO and PPS/REGO composites

PPS is an insulating material (10^{-16} S/cm), which limits its use in self-health monitoring and electro-actuation.[52] The incorporation of carbon nanotubes as conductive fillers is well known to improve PPS electrical conductivity. [24, 51] Herein, EG was used as conductive fillers to improve PPS electrical conductivity for the first time. As shown in Fig. 16, PPS/EGO composite displayed conductivities in the range from 2.26×10^{-3} to 6.8×10^{-3} S/cm with EGO loading increase from 0.5 to 5 wt%. Although the serious REGO reunion were detected in 2-5 wt% PPS/REGO composites, PPS/REGO composites shows the conductivity value is much higher than that the composite reinforced with EGO. As REGO filler content increase from 0.5 to 5 wt%, PPS/REGO composite conductivities rise from 3.42×10^{-3} to 1.17×10^{-2} S/cm. Although EGO was an excellent candidate for enhancing the mechanical behaviors, the oxygen-containing carbons of EGO introduce the structural defects on its surface

which disrupt the electronic continuum medium and reduce composite electrical conductivity. The percolation thresholds of PPS/REGO and PPS/EGO composite was also calculated, and their results were equal to 0.03 wt% ± 0.02 wt% and 0.05 wt% ± 0.04 wt%.[53]

Conclusion

Electrical conductive poly(phenylene sulfide) (PPS)/exfoliated graphite (EG) composites were prepared by 1-chlornaphthalene blending method, and the interface effects between EG and PPS on PPS/EG material properties were well characterized by TEM, SEM, FT-IR, WAXD, DSC, TG, single fiber strength tester technology and four-point probe method. PPS/EGO composite displayed conductivities in the range from 2.26×10^{-3} to 6.8×10^{-3} S/cm with EGO loading increase from 0.5 to 5 wt%. Although the serious REGO reunion were detected in 2-5 wt% PPS/REGO composites, PPS/REGO composites shows the conductivity value is much higher than that the composite reinforced with EGO. As REGO filler content increase from 0.5 to 5 wt%, PPS/EGO composite conductivities rise from 3.42×10^{-3} to 1.17×10^{-2} S/cm. However, EGO is excellent nanofiller for enhancing composite mechanical performance. When 1 wt% EGO was incorporated into PPS, the breaking strength of PPS/EGO achieved maximum 1.3×10^{3} MPa, and this value was 109.5 time as that of pure PPS, which was attributed to the heterogeneous nucleation of EGO and the formation of a large number of covalent bond between PPS and EGO. However, the breaking strength of 5 wt% EGO composite declined to 624 MPa. The excessive addition of fillers reduced PPS crystallization degree and caused the phenomenon of

EGO and REGO aggregation.

When EGO content is less than 3 wt%, PPS/EGO crystallized easily due to the heterogeneous nucleation of EGO. However, EGO content comes up to 5 wt%, PPS/EGO crystallized slower because the intense restrictions on chain mobility are imposed by the EGO-polymer chemical interactions. Be contrary to EGO, REGO only hindered the mobility and diffusion of PPS chains, and the addition of REGO did not promote PPS heterogeneous nucleation. Compared with PPS, PPS/EGO and PPS/REGO displayed the higher thermal stability, and the thermal stability of PPS/EGO was little better than that of PPS/REGO.

Acknowledgements

The authors are grateful for the financial support of the National and Tianjin Natural Science Foundation of China (nos. 21376177, 51173131 and 12JCZDJC29800).

References

1 A.B. Morgan, *Polym Advan Technol 2006*, **17**, 206-217.

2 S. Pavlidou, C. D. Papaspyrides, *Prog Polym Sci* 2008, **33**, 1119-1198.

3 D.G. Brady, *J. Appl. Poly. Sci: Appl Polymer Symp.* 1981, **36**, 231-239.

4 J. E. Frommer, *Acc. Chem. Res.* 1986, **19**, 2-9.

5 J. James, T. Edmonds, J. Harold and W. Hill, US 3354129 A, 1967-03-15.

6 A.M. Diez-Pascual and M. Naffakh, *Composites A* 2013, **54**, 10-19.

7 Z. Spitalsky, D. Tasisb, K. Papagelis and C. Galiotis, *Prog. Polym. Sci.* 2010, **35**, 357-401.

8 A.M. Díez-Pascual and M. Naffakh, *Polymer* 2012, **53**, 2369-2378.

9 A.M. Díez-Pascual, M. Naffakh, C. Marco and G. Ellis, *Composites A* 2012, 43, 603-612.

10 M. Naffakh, A.M. Díez-Pascual, C. Marco and G.J. Ellis. *Mater. Chem.* 2012, **22**, 1418-1425.

11 A.M. Díez-Pascual, M. Naffakh, C. Marco and G. Ellis, *J. Phys. Chem. B* 2012, 116, 7959-7969.

12 A.M. Díez-Pascual and M. Naffakh, ***Carbon*** 2012, **50**, 857-868.

13 A.M. Díez-Pascual and M. Naffakh, *Mater. Chem. Phys.* 2012, **135**,348-357.

14 J.M. Gonzalez-Domınguez, A.P. Castell, S. Bespın-Gascon, A. Anson-Casaos, A.M. Dıez-Pascual, M.A. Gomez-Fatou, A.M. Benito, W.K. Masera and M.T. Martınez, *J. Mater. Chem.* 2012, **22**, 21285-21297.

15 J. In-Yup, L. Hwa-Jeong, S.C. Yeong, T. Loon-Seng and B. Jong-Beom, *Macromolecules* 2008, **41**,7423-7432.

16 S. Bahadur and C. Sunkara. *Wear*, 2005, **258**, 1411-1421.

17 C.J. Schwartz and S. Bahadur. Wear, 2000, **237**, 261-273

18 Y.F. Zhao, M. Xiao, S.J. Wang, X.C. Ge and Y.Z. Meng, *Compos. Sci. Technol.* 2007, **67**, 2528-2534.

19 V.L. Shingankuli, J.P. Jog and V.M. Nadkarni, *J. Appl. Polym. Sci.* 1988, **36**, 335-351.

20 I.H. Lee, S.W. Han and H.J. Cho. *Adv. Mater.* 2001, **13**, 1617-1620.

21 D. Lu and S.W. Pan, *Polym. Eng.* 2006, **46**, 820-825.

22 M.H. Cho and S.A. Bahadur, *Tribol. Lett.* 2007, **25**, 237-245.

23 S. Yu, W.M. Wong, S. Hu and Y.K. Juay, *J. Appl. Polym. Sci*. 2009,**113**, 3477-3483.

24 J. Yang, T. Xu, A. Lu, Q. Zhang, H. Tan and Q. Fu, *Compos. Sci. Technol.* 2009, 69, 147-153.

25 A. Thess, R. Lee, P. Nikolaev, H.J. Dai, P. Petit, J. Robert, C.H. Xu, Y.H. Lee, S.G. Kim, A.G. Rinzler, D.T. Colbert, G.E. Scuseria, D. Tománek, J.E. Fischer and R.E. Smalley. *Science* 1996, **273**, 483-487.

26 K.S. Novoselov, A.K. Geim, S.V. Morozov, D. Jiang, Y. Zhang, S.V. Dubonos, I.V. Grigorieva and A.A. Firsov. Science 2004, **306**, 666-669.

27 A.K. Geim and K.S. Novoselov, *Nat Mater* 2007, 6, 183-191.

28 J.W. Gu, C. Xie, H. Li, J. Dang, W.C. Geng and Q.Y. Zhang. *Polym. Compos.* 2014, **35**, 1087-1092.

29 J.W. Gu, J.J. Du, J. Dang, W.C. Geng, S.H. Hua and Q.Y. Zhang, *RSC Adv.* 2014, **4**, 22101–22105.

30 B. Chenlu, L. Song, C.A. Wilkie, B. Yuan, Y. Guo, Y. Hu and X. Gong, *J. Mater. Chem.* 2012, **22**, 16399-16406.

31 J.F. Shen, B. Yan, M. Shi, H. Ma, N. Li and M. Ye, *J. Mater. Chem.* 2011, **21**, 3415-3421.

32 S. Dubin, S. Gilje, K. Wang, V. Tung, K. Cha, A. Hall, J. Farrar, R. Varshneya, Y. Yang and R.A. Kaner, *ACS Nano* 2010, **4**, 3845-3852.

33 Y. Zhu, S. Murali, W.W. Cai, X.S. Li, J.W. Suk, J.R. Potts and R.S. *Adv. Mater.* 2010, **22**, 3906-3924.

34 B.J. Tabor, E.P. Magre and J. Boon, *Eur. Polym. J.* 1971,**7**, 1127-1133.

35 D.A. Zimmerman, J.L. Koenig and H. Ishida, *Polymer* 1999, **40**, 4723-4731.

36 H.L. Guo, X.F. Wang, Q.Y. Qian, F.B. Wang and X.H. Xia, *ACS Nano.* 2009, **22**, 2653-2659.

37 Z.L. Li, Y.J. Mi, X.L. Liu, S. Liu, S.R Yang and J.Q. Wang, *J Mater Chem* 2011, **21**, 14706-14711.

38 Q. Chang, S. Song, J. Li and J. Ma, *Anal Methods* 2012, **4**, 1110-1116.

39 D. Cai and M. Song. *J. Mater. Chem.* 2010, **20**,7906-7915.

40 S, Watcharotone, D.A. Dikin, S. Stankovich, R. Piner, I. Jung, G.H.B. Dommett, G. Evmenenko, S.E. Wu, S.F. Chen, C.P. Liu, S.T. Nguyen and R.S. *Nano Lett.* 2007. **7**, 1888-1892.

41 S. Park, K.S. Lee, G. Bozoklu, W. Cai, S.T. Nguyen, R.S. Ruoff, ACS Nano 2008, **2**, 572-578.

42 Q.K. Meng, M. Hetzer, D.D. Kee, *J. Compos. Mater,* 2010, **45**, 1145-1158.

43 M. Naffakh, Marco C, M.A. Gomez, I. Jimenez, *J. Phys. Chem*. 2009, **113**,7107-7115.

44 B. Chenlu, L. Song, W. Xing, B. Yuan, C.A. Wilkie, J. Huang, Y. Guo and Y. Hu, *J. Mater. Chem.* 2012, **22**, 6088-6096.

45 T. Kurose, V.E. Yudin, J.U. Otaigbe and V.M. Svetlichnyi, *Polymer* 2007; 48:7130-7138.

46 J.P. Jog, N. Bulakh and V.M. Nadkarni, *Bull. Mater. Sci.* 1994, **17**,1079-1089.

47 K. Fukushima, M. Murariu and G. Camina, *Polym. Eng. Sci.* 2010, **95**, 1063-1076.

48 S. Shenogin, A. Bodapati, L. Xue, R. Ozisik and P. Keblinski, *Appl. Phys. Lett.*

2004, **85**, 2229-2231.

49 X.D. Huang and S.H. Goh, *Macromolecules* 2000, **33**, 8894-8897.

50 P.C. Eklund and A.M. Rao, Fullerene Polymers and Fullerene Polymer Composites. Berlin, Springer, 1999, 3540648941.

51 T.K. Mishra, A. Kumar, V. Verma, K.N. Pandey and V. Kumar, *Compos. Sci. Technol.* 2012, **72**, 1627-1631.

52 S. Yu, W.M. Wong, S. Hu and Y.K. Juay, *J Appl Poly Sci* 2009, **113**, 3477–3483.

53 M. Majidian, C. Grimaldi, A. Pisoni, L. Forro a, A. Magrez, *Carbon*, 2014, **80**, 364-372.